Mutations in PLCδ1 associated with hereditary leukonychia display divergent PIP2 hydrolytic function

Michail Nomikos[1,2]*, Angelos Thanassoulas[3], Konrad Beck[4], Maria Theodoridou[2], Jasmine Kew[2], Junaid Kashir[2,5,6], Brian L. Calver[2], Emily Matthews[2], Pierre Rizkallah[7], Zili Sideratou[3], George Nounesis[3], F. Anthony Lai[2]*

[1]Qatar University, College of Medicine, PO BOX 2713, Doha, Qatar

[2]College of Biomedical and Life Sciences, School of Biosciences, Cardiff University, Cardiff, UK

[3]National Center for Scientific Research "Demokritos", 15310 Aghia Paraskevi, Greece

[4]College of Biomedical and Life Sciences, School of Dentistry, Cardiff University, Cardiff, UK

[5]Alfaisal University, College of Medicine, Riyadh, Saudi Arabia

[6]King Faisal Specialist Hospital & Research Center, Department of Comparative Medicine, Riyadh, Saudi Arabia.

[7]College of Biomedical and Life Sciences, School of Medicine, Cardiff University, Cardiff, UK

*Correspondence to:
M Nomikos: mixosn@yahoo.com or FA Lai: LaiT@cf.ac.uk

Article type   : Original Article

Running title: Altered function of PLCδ1 mutants underlying hereditary leukonychia.

Abbreviations: PLC, Phospholipase C; PLCδ1, Phospholipase C delta 1; HL, Hereditary leukonychia (HL), PIP$_2$, phosphatidylinositol 4,5-bisphosphate; IP$_3$, inositol 1,4,5-

trisphosphate; DAG, Diacylglycerol; PKC, protein kinase C; ER, endoplasmic reticulum; PH, pleckstrin homology; GdmCl, guanidinium chloride; ALS, amyotrophic lateral sclerosis; CHOL, cholesterol; PtdCho, phosphatidylcholine; PtdEtn, phosphatidylethanolamine.

ABSTRACT

Hereditary leukonychia is a rare genetic nail disorder characterized by distinctive whitening of the nail plate of all twenty nails. Hereditary leukonychia may exist as an isolated feature, or in simultaneous occurrence with other cutaneous or systemic pathologies. Associations between hereditary leukonychia and mutations in the gene encoding phospholipase C delta-1 (PLCδ1) have previously been identified. However, the molecular mechanisms underlying PLCδ1-mutations and hereditary leukonychia remain uncharacterized. In the present study, we introduced hereditary leukonychia-linked human PLCδ1 mutations (C209R, A574T and S740R) into equivalent residues of rat PLCδ1 (C188R, A553T and S719R), and investigated their effect upon the biophysical and biochemical properties of the PLCδ1 protein. Our data suggest that these PLCδ1 mutations associated with hereditary leukonychia do not uniformly alter the enzymatic ability of this protein leading to loss/gain of function, but result in significantly divergent enzymatic properties. We demonstrate here for the first time the importance of PLC-mediated calcium (Ca^{2+}) signalling within the manifestation of hereditary leukonychia. PLCδ1 is almost ubiquitous in mammalian cells, which may explain why hereditary leukonychia manifests in association with other systemic pathologies relating to keratin expression.

INTRODUCTION

Hereditary leukonychia (HL) or 'porcelain nails' is a rare genetic nail disorder in which the hands and feet present with a whitening of the nail plate of all 20 nails. HL can co-manifest with cutaneous or systemic pathologies such as keratosis palmoplantaris, severe keratosis pilaris, pili torti, hypotrichosis, koilonychias, renal calculi and hair dysplasia; but also occurs as an isolated feature [1]. While dominant and recessive inheritance has been reported, the pathophysiology and genetic basis of HL remains unclear. Previous genetic analyses have associated HL with mutations in the chromosomal region 3p21.3-p22, and the gene encoding phospholipase C (PLC) delta-1 (PLCδ1) [1-3].

PLCδ1 belongs to the ubiquitous family of PLC enzymes, key components of signal transduction in a wide range of cellular signalling pathways. PLCs hydrolyse the membrane lipid substrate, phosphatidylinositol 4,5-bisphosphate (PIP$_2$) to generate two second messengers, inositol 1,4,5-trisphosphate (IP$_3$) and diacylglycerol (DAG). DAG mediates the activation of protein kinase C (PKC), while IP$_3$ binds to the IP$_3$ receptors (IP$_3$Rs) in the endoplasmic reticulum (ER) membrane which opens the intrinsic cation channel to release calcium ions from intracellular stores [4, 5]. Currently, there are 13 mammalian PLC isozymes, grouped into six classes according to structure and activation mechanism: PLC-beta (PLCβ1–4), PLC-gamma (PLCγ1-2), PLC-delta (PLCδ1, 3, and 4), PLC-epsilon (PLCε), PLC-zeta (PLCζ) and PLC-eta (PLCη1-2) [4, 5]. The δ-type PLCs, δ1, δ3, and δ4, are primarily expressed in mammals. Among these, PLCδ1 is expressed abundantly in most tissues.

PLCδ1 is a multi-domain enzyme, whose 3D-structure has been determined [6] to comprise an N-terminal pleckstrin homology (PH) domain followed by two pairs of EF hand

motifs, the X and Y catalytic domains and a C-terminal C2 domain (Figure 1A). Each domain confers a specific role on the hydrolytic enzyme function of PLCδ1. The PH domain binds both PIP_2 and IP_3, and the PH domain-PIP_2 interaction anchors PLCδ1 to phospholipid membranes, increasing PIP_2 hydrolysis rates [7]. The EF hand domains consist of four helix-loop-helix motifs divided in two pair-wise lobes. Although these domains possess Ca^{2+}-binding residues, also identified in various other Ca^{2+} binding proteins such as calmodulin, the requirement for Ca^{2+} binding to the EF hands is not essential for PLCδ1 function [8].

The first lobe of the PLCδ1 EF hands is involved in Ca^{2+}-independent binding of PLCδ1 to anionic phospholipids [9], while the second lobe is vital for enzymatic activity and structural stability [8]. The PLCδ1 catalytic domain has a unique split triose isomerase (TIM) barrel structure, of which the two halves are termed X and Y. The X and Y regions are joined by the flexible, unstructured, auto-inhibitory XY linker **[10]**, which contains a Ca^{2+} binding site that confers Ca^{2+}-dependent enzymatic activity of PLCδ1 [6]. The C-terminal C2 domain is involved in Ca^{2+}-dependent membrane binding of PLCδ1, interacting with phosphatidylserine to form a C2-Ca^{2+}-phosphatidylserine ternary complex that enhances PLCδ1 enzymatic activity [11].

Immunohistochemical analyses have demonstrated high PLCδ1concentrations within the human nail matrix, suggesting a potential role for PLCδ1 in nail development [1]. Significantly, genome wide analyses of individuals with HL have identified a spectrum of mutations in the PLCδ1 gene [1-3]. However, the mechanism by which these mutations alter the molecular properties of PLCδ1 to cause the leukonychia phenotype is currently unknown. In the present study, we introduce three HL-associated human PLCδ1 mutations (C209R, A574T and S740R) into the rat PLCδ1 (C188R, A553T and S719R; Figure 1A) and evaluate

the impact of these mutations on the biophysical and biochemical properties of PLCδ1. Moreover, we also characterize a PLCδ1 mutation identified in a Pakistani family (S740RfsX19) [3] by incorporating a stop codon 19 amino acids adjacent to the S719R point mutation in rat PLCδ1 and determine how truncation of the C-terminal 18 residues alters PLCδ1function.

RESULTS

PLCδ1 construct expression

To investigate how the C188R, A553T and S719R mutations affects the biophysical and biochemical properties of wild-type PLCδ1 (PLCδ1^{WT}), we prepared the PLCδ1^{WT}, PLCδ1^{C188R}, PLCδ1^{A553T}, and PLCδ1^{S719R} constructs for recombinant prokaryotic expression. An additional PLCδ1 mutant (PLCδ1^{E341A}) served as a negative control, as this causes complete loss of PLCδ1 enzymatic activity [12]. Following successful bacterial protein expression and purification by affinity chromatography, PLCδ1 for each wild-type and mutant protein preparation displayed a single band with apparent molecular mass of ~87 kDa (Fig 1B; left panel), which was also recognized by an anti-PLCδ1 antibody (Fig 1B; right panel).

Biophysical characterisation of PLCδ1 wild type and mutant proteins

Circular dichroism (CD) spectra of wild-type and mutant PLCδ1 protein exhibited high congruence. The extrema at 190 and 208 nm, and shoulder at ~221 nm are indicative of substantial α-helical content (Fig. 2A, B). Spectra recorded in the absence (Fig. 2A) and presence of Ca^{2+} (Fig. 2B) were superimposable, with differences of $|\Delta\varepsilon| < 0.2$ M^{-1}cm^{-1} at λ > 200 nm. De-convolution of spectra resulted in α-helical and β-strand contents of 28-32, and 19-22%, respectively, in excellent agreement with the 29.8% α-helical and 21.4% β-strand

content observed in the combined X-ray structures of the N- and C-terminal regions of rat PLCδ1 (pdb codes 1DJG and 1MAI; [13, 14]), indicating expressed proteins appear to adopt the correct conformation.

To evaluate thermal stability of the purified wild-type and mutant PLCδ1 proteins, the CD signal was monitored at 221 nm at increasing temperatures (Figs. 2C, D). Following transitional onset, all proteins precipitated irreversibly. To estimate their relative thermal stabilities, the CD data were fitted using the van't Hoff equation, assuming a common molar circular dichroism for the completely denatured state. In the absence of Ca^{2+}, the resulting apparent melting temperatures were all ~46.0^{o}C (Fig. 2E). Addition of Ca^{2+} increased the thermal stability by 3-4°C for all samples, except PLCδ1^{A553T}, which remained unaffected (Fig. 2D, E).

The thermodynamic stability of PLCδ1 wild-type and mutant proteins was estimated by employing guanidinium chloride (GdmCl)-induced chemical denaturation and monitoring the consequent changes in their intrinsic fluorescence spectra. A wavelength of 295 nm was used for the selective excitation of the eleven tryptophan residues present in the PLCδ1 molecule. Both the intensity and wavelength of tryptophan residue fluorescence are sensitive to the polarity of their local environment. In the native state, all PLCδ1 samples exhibited an emission maximum at 325 nm, while at 5M GdmCl the unfolded molecules possessed an emission maximum at ~345 nm. This red-shift could render intensity measurements at a fixed wavelength misleading. Therefore, to avoid such issues, the intensity-weighted average emission wavelength was calculated from the collected spectra at each denaturant concentration [15]. Typical intensity-weighted average wavelength *vs.* GdmCl concentration plots for both the PLCδ1 Ca^{2+}-free and Ca^{2+}-rich samples are presented in Figure 3A. In contrast to the thermal denaturation (Fig. 2), the reversibility of the chemical denaturation

profile allows for the extraction of meaningful thermodynamic parameters, using a three-state equilibrium model to analyse the data [16].

The results of the non-linear least squares fits are shown in Figure 3; detailed numerical results are presented in Supplementary Information (Tables 1 & 2). In a Ca^{2+}-free environment all constructs appeared marginally stable, with an energy barrier of 17-20 kJ/mol between the native and the fully unfolded state. No significant reduction of stability due to the mutations was observed (all $\Delta\Delta G$ values <4 kJ/mol). To investigate the effect of Ca^{2+} binding on PLCδ1 stability, experiments were repeated in the same buffer with the addition of 10 mM $CaCl_2$. Except for PLCδ1^{A553T}, all proteins demonstrated a marked increase in stability; PLCδ1^{WT} and PLCδ1^{C188R} were ~3.7 kJ/mol more stable when bound to Ca^{2+}, while for PLCδ1^{S719R} the effect was almost double (~ 7.5 kJ/mol). This stabilizing effect is not manifested by a shift of the chemical denaturation curves towards higher denaturant concentrations (Fig. 3), but as a more cooperative transition from the native to the unfolded state within the same concentration range. In the case of PLCδ1^{A553T}, the free energy change of the chemically-induced unfolding remained unchanged in Ca^{2+}-free and in Ca^{2+}-rich buffer (~18.4 kJ/mol), signifying impaired Ca^{2+} sensitivity caused by the A553T mutation, although the A553 residue is not located in any of the Ca^{2+}-binding sites of PLCδ1. Interestingly, the CD melting profiles of PLCδ1^{WT} and mutant proteins exhibited the same thermostability trends. All samples had a higher melting temperature when bound to Ca^{2+}, except for PLCδ1^{A553T}.

Binding of PLCδ1 mutants to PIP$_2$

To examine the effect of mutations on the binding properties of PLCδ1 to PIP$_2$, we employed a liposome binding assay, utilizing unilamellar liposomes composed of a 4:2:1 mixture of phosphatidylcholine:cholesterol:phosphatidylethanolamine, incorporating either 0 or 1% w/w PIP$_2$ of total lipids. To diminish non-specific protein binding to highly charged lipids, the liposome binding assays were performed in the presence of near-physiological concentrations of MgCl$_2$ (0.5 mM) [17, 18]. PLCδ1^{WT} bound strongly to liposomes containing 1% w/w PIP$_2$ in the presence or absence of Ca^{2+}, but the protein remained in the supernatant in the absence of PIP$_2$. The binding properties of all PLCδ1 mutants (PLCδ1^{C188R}, PLCδ1^{A553T} and PLCδ1^{S719R}) were very similar to PLCδ1^{WT}, interacting strongly with liposomes containing 1% w/w PIP$_2$ regardless of the presence of Ca^{2+} (Fig. 4). These data suggest that none of these mutations alter PLCδ1 binding to PIP$_2$.

Enzymatic characterization of C188R, A553T and S719R mutants

The specific PIP$_2$ hydrolytic activity of each recombinant protein was determined using an *in vitro* [^{3}H]PIP$_2$ hydrolysis assay [19-21]. The enzyme-specific activities are summarized in Figure 5A and Table 1 revealing that the wild-type and S719R exhibited no difference in enzymatic activities. C188R retained ~85% of WT enzymatic activity. In contrast, A553T showed a ~40% increase in its enzymatic activity compared to wild-type PLCδ1 (Table 1). Expectedly, the negative control E341A (a mutant form unable to ligate Ca^{2+} in its active site) appeared enzymatically inactive and did not display any *in vitro* PIP$_2$ hydrolytic activity. To compare enzyme substrate kinetics of the wild-type and PLCδ1 mutants, the K_m for the PIP$_2$ substrate was calculated. The K_m values for PLCδ1^{WT} and PLCδ1^{S719R} were nearly identical. In contrast, the Km for PLCδ1^{C188R} was slightly increased

compared to PLCδ1^{WT}, while the *Km* for PLCδ1^{A553T} was ~2.3-fold lower than that of PLCδ1^{WT} (Table 1) indicating that this mutation increases the *in vitro* affinity of PLCδ1 for its substrate PIP$_2$.

To examine the point mutational impact on the Ca^{2+} sensitivity of PLCδ1 enzyme activity, we assessed the ability of PLCδ1 mutants to hydrolyze [^{3}H]PIP$_2$ at Ca^{2+} concentrations in the 0.1 nM to 0.1 mM range. No significant difference was observed in the Ca^{2+} sensitivity of PIP$_2$ hydrolysis with a very similar EC$_{50}$ value (4.8–5.1 μM) for all four recombinant PLCδ1 proteins (Fig. 5B, Table 1).

Expression and enzymatic characterization of PLCδ1^{S719R}fsX19

PLCδ1^{S719R} did not appear to exert any effect on the structural and biochemical properties of PLCδ1. Thus, to fully characterize this mutation identified in a Pakistani family (p.Ser740ArgfsX19), we generated the equivalent mutation in rat PLCδ1, incorporating a stop codon 19 residues adjacent to the S719R point mutation. Attempts to generate PLCδ1^{S719}fsX19 recombinant protein without a fusion tag proved unsuccessful due to severe solubility issues. Therefore, PLCδ1^{S719}fsX19 was cloned into the pETMM60 vector, and purified as a NusA-6His-fusion protein. We have previously demonstrated that NusA is the most efficient fusion partner for human PLCζ, significantly increasing the expression of soluble recombinant proteins in a bacterial host, *E. coli*, by enhancing their stability [22]. Additionally, we cloned PLCδ1^{WT} into the pETMM60 vector and purified it as NusA-6His-fusion protein for direct comparison with PLCδ1^{S719}fsX19.

Figure 5C shows NusA-PLCδ1^{WT} and NusA-PLCδ1^{S719}fsX19 fusion proteins analysed by SDS–PAGE and immunoblot detection. The major protein band displayed a mobility corresponding to the predicted molecular mass for each construct and these bands were also confirmed by the anti-PLCδ1 antibody. PIP$_2$ hydrolytic enzyme activity was determined using the standard [^{3}H]PIP$_2$ hydrolysis assay. The histogram of Figure 5D summarizes the enzyme-specific activity values obtained for each protein, revealing that NusA-PLCδ1^{S719}fsX19 mutant retained only ~22% of NusA-PLδ1^{WT} enzymatic activity (0.40±0.03 *versus* 1.82±0.06 μmol/min/mg). These data suggest that although PLCδ1^{S719R} does not appear to exert a major effect on PLCδ1 activity, an 18 amino acid truncation from the PLCδ1 C-terminus has a significantly deleterious impact on enzymatic function.

DISCUSSION

Hereditary leuconychia is a rare nail pathology in which patients present with a partial or totally white nail plate. Recent studies provided the first genetic links between PLCδ1 and HL by identifying mutations in the PLCδ1 protein sequence of family members exhibiting characteristic features of HL [1-3]. Both dominant and recessive inheritance is known to underlie manifestation of this nail disorder. Despite the in-depth structural characterization of PLCδ1, the specific physiological role of this enzyme has only recently become more evident through the identification of its contribution to human disease.

PLCδ1 was significantly down-regulated in colorectal- [23], breast- [24], and gastric- [25] cancers, including chronic myeloid leukaemia [26]. More specifically, the PLCδ1 promoter in 79% of analysed colorectal cancer cell lines was methylated, suggesting the potential involvement of PLCδ1 in tumour suppression [23]. Furthermore, PLCδ1 cellular distribution alters in a cell cycle-dependant manner, while suppression of PLCδ1 leads to

increased levels of cyclin E [27], indicating that PLCδ1 may contribute to cell cycle regulation. Studies with transgenic mice suggest a role for PLCδ1 in thermogenesis and adipogenesis, as PLCδ1$^{-/-}$ mice had significantly lower body-weight and -fat mass compared to PLCδ1$^{+/-}$ mice [28]. Moreover, recent evidence has suggested a role for PLCδ1 in the neurodegenerative disease, amyotrophic lateral sclerosis (ALS), as expression of PLCδ1 in SOD1(G93A) mutant mice (animal model of ALS) was significantly up-regulated [29]. Genetic deletion of PLCδ1 in these mice significantly improved survival [29], although the molecular mechanism underlying this process remains unresolved.

Although PLCδ1 is highly expressed in the nail matrix [1] the exact mechanism underlying PLCδ1 mutation leading to leukonychia is currently unclear. Here we have examined the effect of three HL-associated PLCδ1 mutations on the biophysical and enzymatic properties of rat PLCδ1. Additionally, we characterized a novel PLCδ1 mutation identified in a Pakistani family (S740RfsX19) [3], generating the equivalent PLCδ1 mutant in rat PLCδ1 sequence by incorporating a stop codon 19 amino acids downstream of the S719R point mutation.

Within the C209R mutant protein, the relatively small cysteine residue is replaced by the larger, positively-charged arginine residue. Interestingly, attempts to crystallize the first EF hands of PLCδ1 were unsuccessful due to poorly ordered crystals [6, 30], whereas the successful crystallization of the second EF hand suggests that this domain may contribute to the rather rigid core of PLCδ1 [6]. As presented in Fig. 6, the Cys side-chain can be efficiently accommodated inside the hydrophobic interior of the protein. However, the same cannot apply to the much larger Arg side-chain. The presented model shows a contorted configuration to avoid clashes, using χ dihedral rotations. But this may not be a stable fold in

the vicinity. Our experimental observations (Figure 2D) showed that the thermal stability of this mutant is slightly increased compared to PLCδ1^{WT} protein suggesting that even partial unfolding in that part of the fold does not prevent Ca^{2+}binding to the neighbouring EF hand domain. In any case, the Ca^{2+} binding to this EF hand domain appears to be of secondary importance to the main function of the protein, as this mutation exerted little effect on enzymatic Ca^{2+}-sensitivity. Additional mutational analyses revealed that when the proposed Ca^{2+} binding residues are replaced (Asp-153, Asp-157 and Glu-164), the enzymatic activity was not reduced [8], suggesting that Ca^{2+}-binding to this EF hand may not be part of a PLCδ1 regulatory mechanism.

The S719R (human: PLCδ1^{S740R}) mutation did not exert a significant effect on the biophysical and biochemical properties of PLCδ1. The small side-chain of Ser-719 points into an open groove created by neighbouring side-chains (Fig 6) that is large enough to accomodate the large Arg side-chain with appropriate χ dihedral rotations to avoid clashes. The distal guanidinium group emerges into the solvent region, displacing solvent molecules found in the 1DJH structure, on which this model is based. Neighbouring active site domains are not significantly altered by this mutation. Contrastingly, although the S719R mutation did not affect enzymatic activity, truncation of the remaining 18 amino acids from the C-terminus exerted deleterious effects on PLCδ1 stability and activity. This major dysfunction in the hydrolytic activity of the PLCδ1 protein consequently leads to the leukonychia phenotype in the Pakistani family carrying the S740RfsX19 mutation [3].

The most intriguing mutational effects were observed for the A553T (human: A574T) mutation occurring in the Y-domain (residues 489-606). Replacement of the small hydrophobic alanine side chain with the polar, hydrophilic threonine significantly increased catalytic activity. The Ala side-chain is completely enveloped inside the hydrophobic core of

the fold with optimal van der Waals distances to neighbouring residues (Fig 6). A Thr side-chain is larger, and polar, causing steric hindrance in at least one location. The precise effect is not known without structure determination, but it can be envisaged that the strain is relieved by appropriate main/side-chain rearrangement in the vicinity to accommodate the residue change. It is plausible that these changes make for a different binding mode of the substrate, making it more available for the reaction, thus increasing enzymatic activity. It is also worth noting that although the A553T mutation is located in the Y domain, which has intact Ca^{2+} binding site, the presence of Ca^{2+} ion does not increase its thermal stability (Figure 2D). This suggests that A553T mutation, which is located close to the surface, has a significant impact on the fold stability in the presence of Ca^{2+} ion, without affecting the enzymatic properties of this protein (Figures 5A, B).

Prior to studies implicating the involvement of mutations in the 3p21.3-p22 chromosomal region, only one other genetic linkage study investigated the autosomal dominant leukonychia that displayed no other related abnormalities [31]. This study concluded that mutations in the 12q13 region, encoding type II cytokeratins and hard keratins, were associated with HL [31]. Together with the more recent evidence implicating PLCδ1 mutants in HL, an aberrant *PLCD1* gene may lead to altered keratin expression resulting in a leukonychia phenotype. Support for this hypothesis arises from data showing that PLCδ1 expression can be induced by the *Foxn1* transcription factor involved in the regulation of hair keratin expression [32]. Nude mice with mutated *Foxn1* presented with reduced PLCδ1 levels in hair follicles, suggesting that *Foxn1* is an upstream regulator of PLCδ1 expression and decreased PLCδ1 protein results in abnormal hair follicles and the hairless phenotype seen in *Foxn1* mutant 'nude' mice. However, further investigations are

required to understand the precise molecular mechanisms linking the *PLCD1* gene with pathogenesis of HL in humans.

Our findings suggest that PLCδ1 mutations associated with HL do not uniformly alter activity, but instead results in divergent enzymatic function, that produces either increase, decrease or no change in ability to hydrolyse the phospholipid substrate, PIP$_2$. Moreover, PLCδ1 is almost ubiquitous in mammalian cells and hence genetic mutations in this gene would alter the activity of the protein in all cell types. Indeed, the ubiquitous presence of PLCδ1 might explain why HL may also manifest in association with other systemic pathologies relating to keratin expression. However, as the specific physiological role of PLCδ1 in different cell types is not fully understood, it is not clear why it is only the nails that are affected. We demonstrate here for the first time the importance of PLC-mediated Ca^{2+} signaling within the manifestation of HL, warranting further detailed investigations to elucidate such mechanisms in order to fully understand the molecular pathology of such manifestations.

MATERIALS AND METHODS

Plasmid construction

Rat PLCδ1 (GenBank accesion number M20637) in the pGEX-5X2 plasmid [20] was subjected to site-directed mutagenesis (QuikChange II; Stratagene) to generate the PLCδ1^{C188R}, PLCδ1^{E341A}, PLCδ1^{A553T} and PLCδ1^{S719R} mutants. Each construct was confirmed by dideoxynucleotide sequencing (Applied Biosystems Big-Dye Ver 3.1 chemistry and model 3730 automated capillary DNA sequencer by DNA Sequencing & Services^{TM}). Wild type PLCδ1 (PLCδ1^{WT}) and the aforementioned PLCδ1 mutants were amplified by PCR from the pGEX-5X2-PLCδ1 plasmid using Phusion polymerase

(Finnzymes), and the appropriate primers to incorporate 5'-SalI and 3'-NotI sites. PLCδ1[WT] and mutants were then cloned into the pHSIE vector. The primers used for the amplification were: 5'-ACCAGTCGACATGGACTCGGGTAGGGACTTCC-3' (forward) and 5'-GAGAGCGGCCGCTCAGTCCTGGATGGAGATCTTCAC-3' (reverse).

For the pETMM60-PLCδ1[S719]fsX19 deletion construct, PLCδ1[S719]fsX19 was amplified by PCR from the pGEX-5X2-PLCδ1[S719] plasmid using Phusion polymerase (Finnzymes) and the appropriate primers to incorporate 5'-SalI and 3'-NotI sites. PLCδ1[WT] and mutants were then cloned into the pETMM60 vector. The primers used for the amplification were: 5'-ACCAGTCGACATGGACTCGGGTAGGGACTTCC-3' (forward) and 5'- GAGAGCGGCCGCTCACTTAGACAAGAGGTGGACATGG-3' (reverse). pETMM60-PLCδ1[WT] has been generated previously [18].

Protein expression and purification

For 6xHis-SUMO2-intein-PLCδ1-fusion protein expression, *Escherichia coli* [BL21-CodonPlus(DE3)-RILP; Stratagene], transformed with the appropriate plasmid, was cultured at 37 °C until the A_{600} nm reached 0.6. Protein expression was induced for 18 h at 16°C with 0.2 mM IPTG (isopropyl β-D-thiogalactopyranoside), (ForMedium). Bacterial cell pellets were harvested by centrifugation at 6,000 g for 15 minutes, 4°C and then recombinant PLCδ1 proteins were purified as previously described [33].

For NusA-6xHis-fusion protein expression, *Escherichia coli* [BL21-CodonPlus(DE3)-RILP; Stratagene], transformed with the appropriate pETMM60-PLCδ1 plasmid, was cultured at 37 °C until A600 reached 0.6, and protein expression was induced for 18 h at 16°C with 0.1 mM IPTG (ForMedium). Cells were harvested (6000 g for 15 min), resuspended in phosphate-

buffered saline (PBS) containing protease inhibitor mixture (EDTA-free; Roche) and sonicated 4 x15 seconds on ice. Soluble NusA-6xHis fusion PLCδ1 protein was purified on Ni-NTA resin following standard procedures (Qiagen) and eluted with 275 mM imidazole. Eluted proteins were dialysed overnight (10 000 MWCO; Pierce) at 4°C against 4 l of PBS.

SDS-PAGE and western blotting

Recombinant proteins were separated by SDS-PAGE as previously described [22]. Separated proteins were transferred onto polyvinylidene difluoride membranes (Immobilon-P; Millipore) using a semi-dry transfer system (Trans-Blot SD; Bio-Rad) in buffer (48 mM Tris, 39 mM glycine, 0.0375% w/v SDS, 20% v/v methanol) at 20 V for 1 hour. Membranes were incubated overnight at 4°C in Tris-buffered saline, 0.1% v/v Tween 20 (TBS-T) containing 5% w/v non-fat milk powder, and probed with anti-PLCδ1 rabbit polyclonal antibody (1:5,000 dilution; Santa Cruz). Detection of horseradish peroxidase-coupled secondary antibody was achieved using enhanced chemiluminescence detection (ECL; Amersham Biosciences).

**Circular dichroism (CD) spectroscopy and thermal denaturation measurements**

CD data were acquired on an Aviv 215 spectrophotometer (Aviv Biomedical Inc., Lakewood, NJ). Before measurements, protein samples in 50 mM KCl, 10 mM MES, pH 6.5, including either 1 mM EDTA or 1 mM CaCl$_2$ were centrifuged at 14,000 x g for 30 min. Far-UV spectra (~185-260 nm) were collected in a 0.02 cm quartz cell at 4°C at protein concentrations of ~5 μM with an 8s accumulation time in 0.2 nm intervals, using a 1 nm bandwidth and buffer baselines were subtracted. Protein concentrations were determined from the absorption at 280 nm, assuming extinction coefficients calculated based on the amino acid composition [34]. CD spectra were deconvoluted for the secondary structure

content using the CDsstr algorithm [35] as implemented in the Dichroweb server [36] with the SP175 reference data set [37]. Thermal denaturation curves ($c_{protein}$ = 2 µM; 0.1 cm pathlength cell) were recorded at 221 nm in 0.5 $^{\circ}$C intervals from 4 to ~60°C with settings resulting in an average heating rate of *ca*. 30 $^{\circ}$C/h. As all proteins precipitated irreversibly upon unfolding, the onset of the transition curves were fitted to an extension of the van't Hoff equation assuming a two-state transition from the native to the unfolded conformation to establish apparent melting temperatures (T_m). For the unfolded conformation, a molar circular dichroism $\Delta\epsilon$ of -1.3 $M^{-1}cm^{-1}$ as previously reported for various thermally denatured protein [38] was assumed as a constant.

Chemical denaturation and fluorescence measurements

The equilibrium unfolding of PLCδ1 wild type and mutant forms was studied by monitoring changes in their intrinsic fluorescence as a function of guanidine hydrochloride concentration (GdmCl). After exciting the sample at 295 nm, fluorescence emission spectra from 300 to 450 nm were recorded using a QuantaMaster UV Vis spectrofluorometer (Photon Technology International, Inc. Birmingham, UK). Experiments were performed at 20˚C, and the slit widths were set at 1 nm for excitation and 3 nm for emission. Samples at a protein concentration of 1 µM were incubated for 24 h before taking measurements to ensure that equilibrium was reached. To minimize bleaching effect, a scan rate of 2 nm/sec was used, with a band pass for both excitation and emission at 2 nm. Spectra were corrected for background contribution, and an intensity-weighted average emission wavelength was computed at each denaturant concentration. All measurements were repeated at least three times.

Gibbs free energy changes for the chemically-induced protein unfolding transition were determined using a three state equilibrium thermodynamic model:

$$N \underset{\longleftarrow}{\overset{K_{NI}}{\longrightarrow}} I \underset{\longleftarrow}{\overset{K_{IU}}{\longrightarrow}} U$$
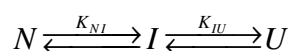
where N, I and U are the native, intermediate and unfolded states of the protein, respectively. The experimental data were plotted as intensity-weighted average emission wavelength change (using the native state as reference) versus the GdmCl concentration of the sample and analyzed by nonlinear least-squares fitting of a two-step unfolding function:

$$F_U = \frac{K_{NI}K_{IU}}{1 + K_{NI} + K_{NI}K_{IU}} \quad Y_{total} = Y_N + F_I \cdot (Y_I - Y_N) + F_U \cdot (Y_U - Y_N)$$

where:

$$Y_N = a_N + b_N \cdot [D], \quad Y_U = a_U + b_U \cdot [D]$$

$$RT \ln K_{NI} = m_{NI}[D] - \Delta G_{NI}, \quad RT \ln K_{IU} = m_{IU}[D] - \Delta G_{IU},$$

$$F_N = \frac{1}{1 - K_{NI} + K_{NI}K_{IU}}, \quad F_I = \frac{K_{NI}}{1 + K_{NI} + K_{NI}K_{IU}}, \quad F_U = \frac{K_{NI}K_{IU}}{1 + K_{NI} + K_{NI}K_{IU}}.$$

Y_{total} is the observed intensity-weighted average emission wavelength change, Y_N, Y_I, and Y_U are the intensity-weighted average emission wavelengths of native, intermediate and unfolded states respectively, [D] is the GdmCl concentration, α_N is the signal at the native state at 0M denaturant, β_N is the signal slope ($d\alpha_N/d[D]$) at the native state, α_U and β_U are the corresponding quantities for the unfolded state. ΔG_{NI} is the difference in Gibbs' free energy of native and intermediate state, and ΔG_{IU} is the difference between intermediate and unfolded state. m_{NI} is a proportionality constant related to the average degree of exposure of residues between the native and the intermediate state, while the parameter m_{IU} has the same physical meaning for the transition from the intermediate to the unfolded state.

Fluorescence data were analysed using Origin software (OriginLab, Northampton, MA).

Liposome preparation and binding assay

Unilamellar liposomes were prepared as previously described [17, 18] by the extrusion method using a laboratory extruder (LiposoFast-Pneumatic, Avestin Inc., Ottawa, ON, Canada) with lipids purchased from Avanti Polar Lipids Inc. (Alabaster, AL). In a typical experiment for preparing a 2 ml dispersion of liposomes, 0.038 mmol (19×10^{-3} M) 1,2-dipalmitoyl*sn*- glycero-3-phosphocholine (PtdCho), 0.019 mmol (9.5×10^{-3} M) of cholesterol (CHOL; molar ratio of PtdCho:CHOL 2:1), 0.0095 mmol (4.8×10^{-3} M) 1,2-dimyristoyl-*sn*-glycero-3-phosphoethanolamine (PtdEtn; molar ratio of PtdCho:PtdEtn 4:1) and 1% of total lipids 1,2-Diacyl-sn-glycero-3-phospho-(1-D-myo-inositol 4,5-bisphosphate) sodium salt (PIP2) were dissolved in a chloroform:methanol solution (2:1 v/v) for the formation of lipid films. The film was hydrated with 2 ml of PBS and the resultant suspension was extruded through two-stacked polycarbonate filters of 100 nm pore size. Twenty-five cycles of extrusion were applied at 50°C. For the control experiments, unilamellar liposomes without PIP2 were prepared in an analogous manner. Dynamic light scattering (DLS) was employed to determine the size of the liposomes, which used a light scattering apparatus (AXIOS–150/EX, Triton Hellas, Thessaloniki, Greece) with a 30 mW laser source and an Avalanche photodiode detector set at a 90° angle. DLS measurements of the extruded lipid preparation showed a narrow monomodal size distribution with average liposome diameter of 100 nm and a polydispersity index of 0.20–0.25. For protein-binding studies, liposomes (100 mg of 4:2:1 PtdCho:CHOL:PtdEtn) containing 0–1% w/w PIP_2 were incubated with 1 mg of recombinant protein for 30 minutes at room temperature in the presence of 1mM of $CaCl_2$ or 1mM of EDTA, and centrifuged for 5 hours at 4°C. The supernatant and pellet were then analysed by SDS-PAGE and Coomassie Blue staining.

Assay of PLC activity

PIP$_2$ hydrolytic activity of recombinant PLC proteins was assayed as described previously [19, 20]. The final concentration of PIP$_2$ in the reaction mixture was 220 μM, containing 0.05 μCi of [^{3}H]PIP$_2$. The assay conditions were optimized for linearity, requiring a 20-min incubation of 200 pmol of PLCδ1 protein sample at 37°C. In assays examining the Ca^{2+} sensitivity, Ca^{2+} buffers were prepared by EGTA/CaCl$_2$ admixture, as described previously [17]. K_m and EC$_{50}$ values of Ca^{2+} dependence for PIP$_2$ hydrolysis for PLCδ1 recombinant proteins were determined by non-linear regression analysis (GraphPad Prism 6). Five PIP2 concentrations were used for the K_m estimation of wild type PLCδ1 and mutants; 2.2, 22, 55, 110 and 220 μM. For these experiments the number of repeats was 4 (n=4), using two different preparations of recombinant protein.

Molecular modeling

PDB entry 1DJH from the PDB database was used as a starting model. The program COOT was used to mutate the side chains of Cys 188 to Arg, Ala 553 to Thr and Ser 719 to Arg. The modified side chains were fitted by rotations around the χ dihedrals to avoid obvious clashes. No other adjustments were made and no molecular dynamics runs were conducted.

AUTHOR CONTRIBUTIONS

M.N., G.N. and F.A.L. devised the project strategy. M.N., K.B., G.N. and F.A.L. designed/analyzed the experiments, which were performed by M.N., A.T., K.B., M.T. J. K., J. K., B.L.C, E.M., P.R. and Z.S. M.N. prepared the first manuscript draft, which was revised and approved by all authors.

FUNDING

REFERENCES

1. Kiuru M, Kurban M, Itoh M, Petukhova L, Shimomura Y, Wajid M & Christiano AM (2011) Hereditary leukonychia, or porcelain nails, resulting from mutations in PLCD1. *Am J Hum Genet* **88**, 839-844, doi: 10.1016/j.ajhg.2011.05.014
S0002-9297(11)00207-2 [pii].
2. Farooq M, Kurban M, Abbas O, Obeidat O, Fujikawa H, Kibbi AG, Fujimoto A & Shimomura Y (2012) A novel mutation in the PLCD1 gene, which leads to an aberrant splicing event, underlies autosomal recessive leuconychia. *Br J Dermatol* **167**, 946-949, doi: 10.1111/j.1365-2133.2012.10962.x.
3. Mir H, Khan S, Arif MS, Ali G, Wali A, Ansar M & Ahmad W (2012) Mutations in the gene phospholipase C, delta-1 (PLCD1) underlying hereditary leukonychia. *Eur J Dermatol* **22**, 736-739, doi: 10.1684/ejd.2012.1852
ejd.2012.1852 [pii].
4. Suh PG, Park JI, Manzoli L, Cocco L, Peak JC, Katan M, Fukami K, Kataoka T, Yun S & Ryu SH (2008) Multiple roles of phosphoinositide-specific phospholipase C isozymes. *BMB Rep* **41**, 415-434.
5. Kadamur G & Ross EM (2013) Mammalian phospholipase C. *Annu Rev Physiol* **75**, 127-154, doi: 10.1146/annurev-physiol-030212-183750.
6. Essen LO, Perisic O, Cheung R, Katan M & Williams RL (1996) Crystal structure of a mammalian phosphoinositide-specific phospholipase C delta. *Nature* **380**, 595-602, doi: 10.1038/380595a0.
7. Lomasney JW, Cheng HF, Wang LP, Kuan Y, Liu S, Fesik SW & King K (1996) Phosphatidylinositol 4,5-bisphosphate binding to the pleckstrin homology domain of phospholipase C-delta1 enhances enzyme activity. *J Biol Chem* **271**, 25316-25326.
8. Nakashima S, Banno Y, Watanabe T, Nakamura Y, Mizutani T, Sakai H, Zhao Y, Sugimoto Y & Nozawa Y (1995) Deletion and site-directed mutagenesis of EF-hand domain of phospholipase C-delta 1: effects on its activity. *Biochem Biophys Res Commun* **211**, 365-369.
9. Cai J, Guo S, Lomasney JW & Roberts MF (2013) Ca2+-independent binding of anionic phospholipids by phospholipase C delta1 EF-hand domain. *J Biol Chem* **288**, 37277-37288, doi: 10.1074/jbc.M113.512186
M113.512186 [pii].

10.   Hicks SN, Jezyk MR, Gershburg S, Seifert JP, Harden TK & Sondek J (2008) General and versatile autoinhibition of PLC isozymes. *Mol Cell* **31**, 383-394, doi: 10.1016/j.molcel.2008.06.018 S1097-2765(08)00463-2 [pii].

11.   Lomasney JW, Cheng HF, Roffler SR & King K (1999) Activation of phospholipase C delta1 through C2 domain by a Ca(2+)-enzyme-phosphatidylserine ternary complex. *J Biol Chem* **274**, 21995-22001.

12.   Okada M, Ishimoto T, Naito Y, Hirata H & Yagisawa H (2005) Phospholipase Cdelta1 associates with importin beta1 and translocates into the nucleus in a Ca2+-dependent manner. *FEBS Lett* **579**, 4949-4954, doi: S0014-5793(05)00951-8 [pii]
10.1016/j.febslet.2005.07.082.

13.   Ferguson KM, Lemmon MA, Schlessinger J & Sigler PB (1995) Structure of the high affinity complex of inositol trisphosphate with a phospholipase C pleckstrin homology domain. *Cell* **83**, 1037-1046, doi: 0092-8674(95)90219-8 [pii].

14.   Essen LO, Perisic O, Lynch DE, Katan M & Williams RL (1997) A ternary metal binding site in the C2 domain of phosphoinositide-specific phospholipase C-delta1. *Biochemistry* **36**, 2753-2762, doi: 10.1021/bi962466bi962466t [pii].

15.   Royer CA (1995) Fluorescence spectroscopy. *Methods Mol Biol* **40**, 65-89, doi: 10.1385/0-89603-301-5:65.

16.   Ekblad CM, Wilkinson HR, Schymkowitz JW, Rousseau F, Freund SM & Itzhaki LS (2002) Characterisation of the BRCT domains of the breast cancer susceptibility gene product BRCA1. *J Mol Biol* **320**, 431-442, doi: S0022-2836(02)00478-3 [pii].

17.   Nomikos M, Elgmati K, Theodoridou M, Calver BL, Nounesis G, Swann K & Lai FA (2011) Phospholipase Czeta binding to PtdIns(4,5)P2 requires the XY-linker region. *J Cell Sci* **124**, 2582-2590, doi: 10.1242/jcs.083485
jcs.083485 [pii].

18.   Theodoridou M, Nomikos M, Parthimos D, Gonzalez-Garcia JR, Elgmati K, Calver BL, Sideratou Z, Nounesis G, Swann K & Lai FA (2013) Chimeras of sperm PLCzeta reveal disparate protein domain functions in the generation of intracellular Ca2+ oscillations in mammalian eggs at fertilization. *Mol Hum Reprod* **19**, 852-864, doi: 10.1093/molehr/gat070
gat070 [pii].

19.   Katan M & Parker PJ (1987) Purification of phosphoinositide-specific phospholipase C from a particulate fraction of bovine brain. *Eur J Biochem* **168**, 413-418.

20.   Nomikos M, Blayney LM, Larman MG, Campbell K, Rossbach A, Saunders CM, Swann K & Lai FA (2005) Role of phospholipase C-zeta domains in Ca2+-dependent phosphatidylinositol 4,5-bisphosphate hydrolysis and cytoplasmic Ca2+ oscillations. *J Biol Chem* **280**, 31011-31018, doi: M500629200 [pii]
10.1074/jbc.M500629200.

21.   Nomikos M, Elgmati K, Theodoridou M, Calver BL, Cumbes B, Nounesis G, Swann K & Lai FA (2011) Male infertility-linked point mutation disrupts the Ca2+ oscillation-inducing and PIP(2) hydrolysis activity of sperm PLCzeta. *Biochem J* **434**, 211-217, doi: 10.1042/BJ20101772
BJ20101772 [pii].

22.   Nomikos M, Yu Y, Elgmati K, Theodoridou M, Campbell K, Vassilakopoulou V, Zikos C, Livaniou E, Amso N, Nounesis G, et al. (2013) Phospholipase Czeta rescues failed oocyte activation in a prototype of male factor infertility. *Fertil Steril* **99**, 76-85, doi: 10.1016/j.fertnstert.2012.08.035
S0015-0282(12)02123-1 [pii].

23.   Danielsen SA, Cekaite L, Agesen TH, Sveen A, Nesbakken A, Thiis-Evensen E, Skotheim RI, Lind GE & Lothe RA (2011) Phospholipase C isozymes are deregulated in colorectal cancer--insights gained from gene set enrichment analysis of the transcriptome. *PLoS One* **6**, e24419, doi: 10.1371/journal.pone.0024419
PONE-D-11-09328 [pii].

24.   Xiang T, Li L, Fan Y, Jiang Y, Ying Y, Putti TC, Tao Q & Ren G (2010) PLCD1 is a functional tumor suppressor inducing G(2)/M arrest and frequently methylated in breast cancer. *Cancer Biol Ther* **10**, 520-527, doi: 10.4161/cbt.10.5.12726

12726 [pii].

25.   Hu XT, Zhang FB, Fan YC, Shu XS, Wong AH, Zhou W, Shi QL, Tang HM, Fu L, Guan XY, et al. (2009) Phospholipase C delta 1 is a novel 3p22.3 tumor suppressor involved in cytoskeleton organization, with its epigenetic silencing correlated with high-stage gastric cancer. *Oncogene* **28**, 2466-2475, doi: 10.1038/onc.2009.92

onc200992 [pii].

26.   Song JJ, Liu Q, Li Y, Yang ZS, Yang L, Xiang TX, Ren GS & Chen JB (2012) Epigenetic inactivation of PLCD1 in chronic myeloid leukemia. *Int J Mol Med* **30**, 179-184, doi: 10.3892/ijmm.2012.970.

27.   Kaproth-Joslin KA, Li X, Reks SE & Kelley GG (2008) Phospholipase C delta 1 regulates cell proliferation and cell-cycle progression from G1- to S-phase by control of cyclin E-CDK2 activity. *Biochem J* **415**, 439-448, doi: 10.1042/BJ20080233

BJ20080233 [pii].

28.   Hirata M, Suzuki M, Ishii R, Satow R, Uchida T, Kitazumi T, Sasaki T, Kitamura T, Yamaguchi H, Nakamura Y, et al. (2011) Genetic defect in phospholipase Cdelta1 protects mice from obesity by regulating thermogenesis and adipogenesis. *Diabetes* **60**, 1926-1937, doi: 10.2337/db10-1500

db10-1500 [pii].

29.   Staats KA, Van Helleputte L, Jones AR, Bento-Abreu A, Van Hoecke A, Shatunov A, Simpson CL, Lemmens R, Jaspers T, Fukami K, et al. (2013) Genetic ablation of phospholipase C delta 1 increases survival in SOD1(G93A) mice. *Neurobiol Dis* **60**, 11-17, doi: 10.1016/j.nbd.2013.08.006

S0969-9961(13)00227-1 [pii].

30.   Grobler JA, Essen LO, Williams RL & Hurley JH (1996) C2 domain conformational changes in phospholipase C-delta 1. *Nat Struct Biol* **3**, 788-795.

31.   Norgett EE, Wolf F, Balme B, Leigh IM, Perrot H, Kelsell DP & Haftek M (2004) Hereditary 'white nails': a genetic and structural study. *Br J Dermatol* **151**, 65-72, doi: 10.1111/j.1365-2133.2004.05994.x

BJD5994 [pii].

32.   Nakamura Y, Ichinohe M, Hirata M, Matsuura H, Fujiwara T, Igarashi T, Nakahara M, Yamaguchi H, Yasugi S, Takenawa T, et al. (2008) Phospholipase C-delta1 is an essential molecule downstream of Foxn1, the gene responsible for the nude mutation, in normal hair development. *Faseb J* 22, 841-849, doi: fj.07-9239com [pii]

10.1096/fj.07-9239com.

33.   Wang Z, Li N, Wang Y, Wu Y, Mu T, Zheng Y, Huang L & Fang X (2012) Ubiquitin-intein and SUMO2-intein fusion systems for enhanced protein production and purification. *Protein Expr Purif* 82, 174-178, doi: 10.1016/j.pep.2011.11.017

S1046-5928(11)00344-5 [pii].

34.   Pace CN, Vajdos F, Fee L, Grimsley G & Gray T (1995) How to measure and predict the molar absorption coefficient of a protein. *Protein Sci* **4**, 2411-2423, doi: 10.1002/pro.5560041120.

35.   Johnson WC (1999) Analyzing protein circular dichroism spectra for accurate secondary structures. *Proteins* **35**, 307-312, doi: 10.1002/(SICI)1097-0134(19990515)35:3<307::AID-PROT4>3.0.CO;2-3 [pii].

36.   Whitmore L & Wallace BA (2008) Protein secondary structure analyses from circular dichroism spectroscopy: methods and reference databases. *Biopolymers* **89**, 392-400, doi: 10.1002/bip.20853.

37.   Lees JG, Miles AJ, Wien F & Wallace BA (2006) A reference database for circular dichroism spectroscopy covering fold and secondary structure space. *Bioinformatics* **22**, 1955-1962, doi: btl327 [pii]

10.1093/bioinformatics/btl327.

38.   Venyaminov S, Baikalov IA, Shen ZM, Wu CS & Yang JT (1993) Circular dichroic analysis of denatured proteins: inclusion of denatured proteins in the reference set. *Anal Biochem* **214**, 17-24, doi: S0003269783714508 [pii].

Tables

Table 1

PLC protein	PIP$_2$ hydrolysis enzyme activity (nmol/min$^/$mg)	K_m (µM)	Ca^{2+}-dependence EC$_{50}$ (µM)
PLCδ1^{WT}	1520±40	157±37	5.12±0.04
PLCδ1^{C188R}	1300±30	190±45	5.02±0.04
PLCδ1^{A553T}	2120±70	68±11	4.41±0.04
PLCδ1^{S719R}	1520±50	150±39	4.83±0.05

TABLE LEGENDS

Table 1. *In vitro* enzymatic properties of PLCδ1 mutants. Summary of specific enzyme activity, *Km* and EC$_{50}$ values of Ca^{2+}-dependence for PIP$_2$ hydrolysis, determined by non-linear regression analysis (GraphPad Prism 6), (see Fig. 5A,B).
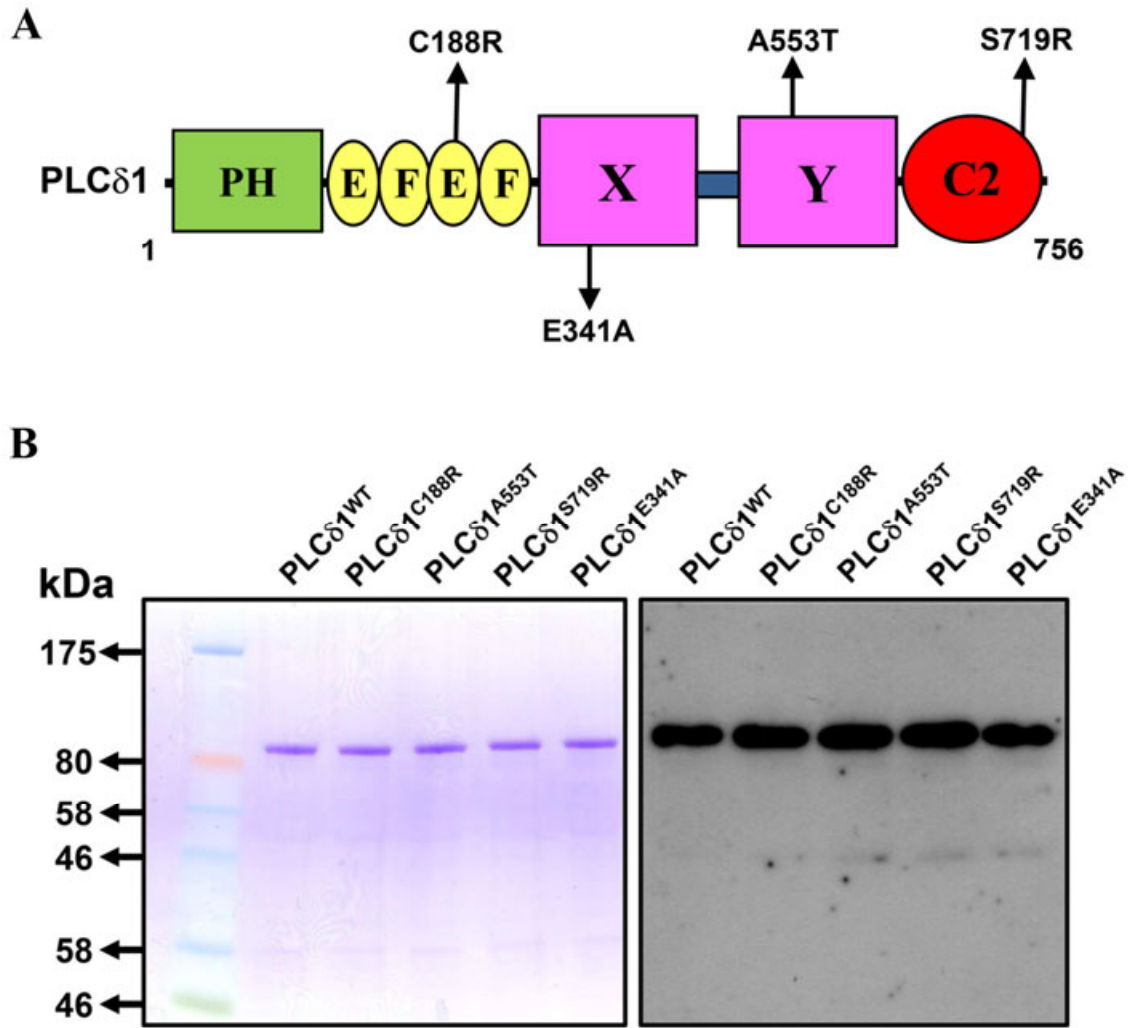
Figure 1. (A) Schematic representation of the PLCδ1 domain structure. PLCδ1 consists of an N-terminal PH domain, two EF hand motifs (EF), catalytic domains X and Y, and a C-terminal domain (C2). The position of the three leukonychia-associated mutations (numbering according to the rat sequence) C188R, A553T and S719R, as well as the E341A control mutation in the X domain are indicated by arrows. **(B)** Expression of recombinant wild type PLCδ1 and mutant proteins. Affinity-purified PLCδ1 proteins (1 µg) were analysed by SDS–PAGE followed by either Coomassie Brilliant Blue staining (left panel) or immunoblot analysis using an anti-PLCδ1 polyclonal antibody at 1:5,000 dilution (right panel).
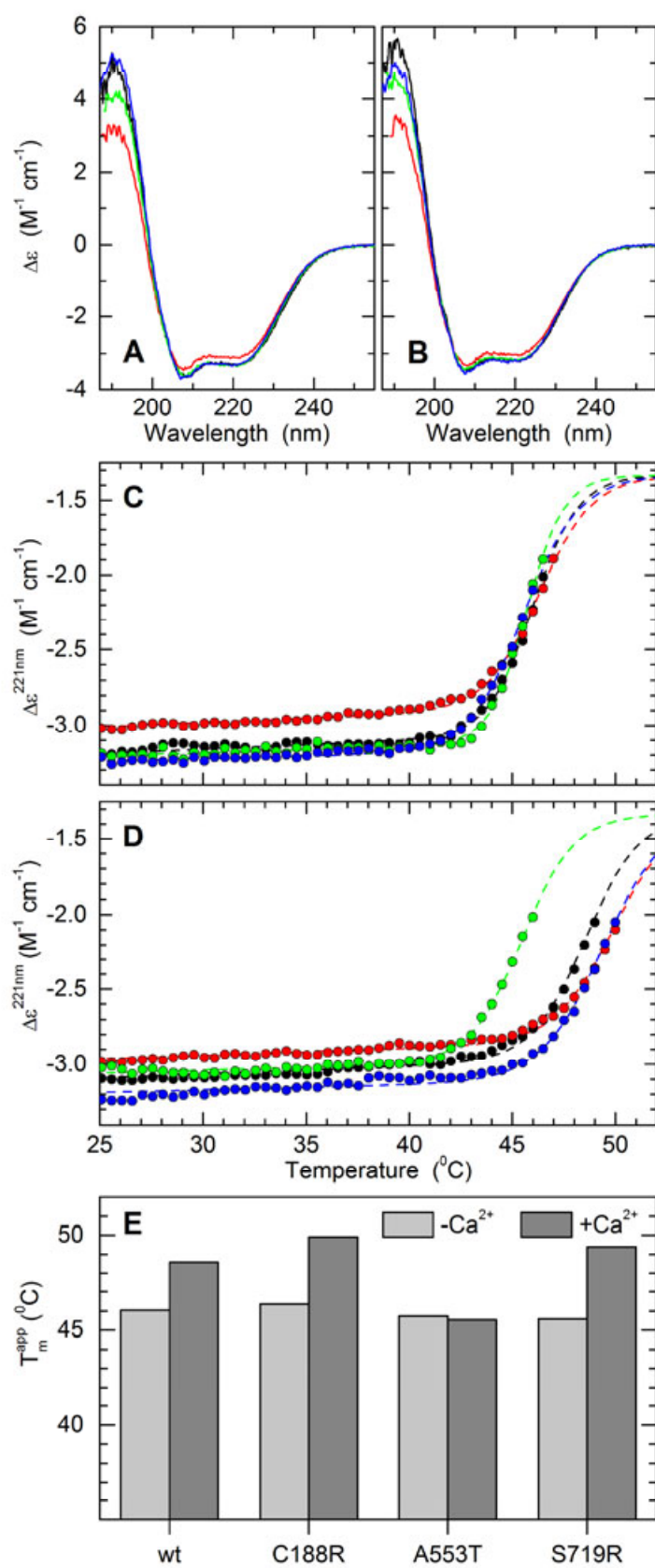
Figure 2. Analysis of secondary structure and thermal stability. CD spectra of PLCδ1 wild type (black) and PLCδ1 mutant proteins C188R (red), A553T (green) and S719R (blue) were recorded at 4°C in the presence of 1mM EDTA (**A**) or 1 mM CaCl$_2$ (**B**). Melting curves were recorded at 221 nm in the presence of 1mM EDTA (**C**) or 1 mM CaCl$_2$ (**D**). Data were fitted (dashed lines) assuming a 2-state transition using the van't Hoff equation. Resultant apparent melting temperatures are shown in **E**.
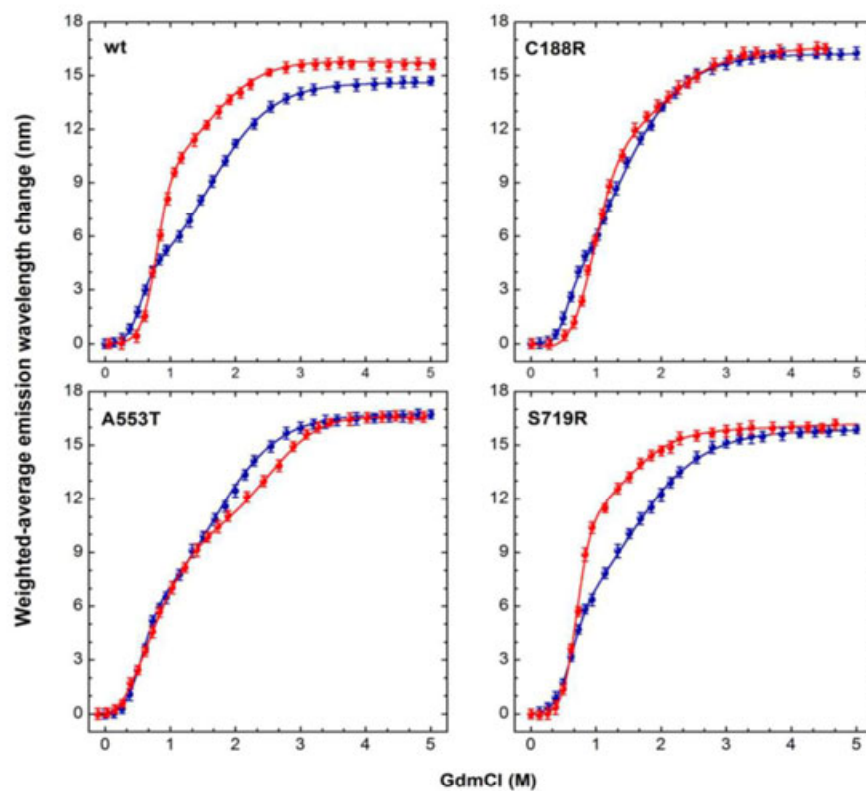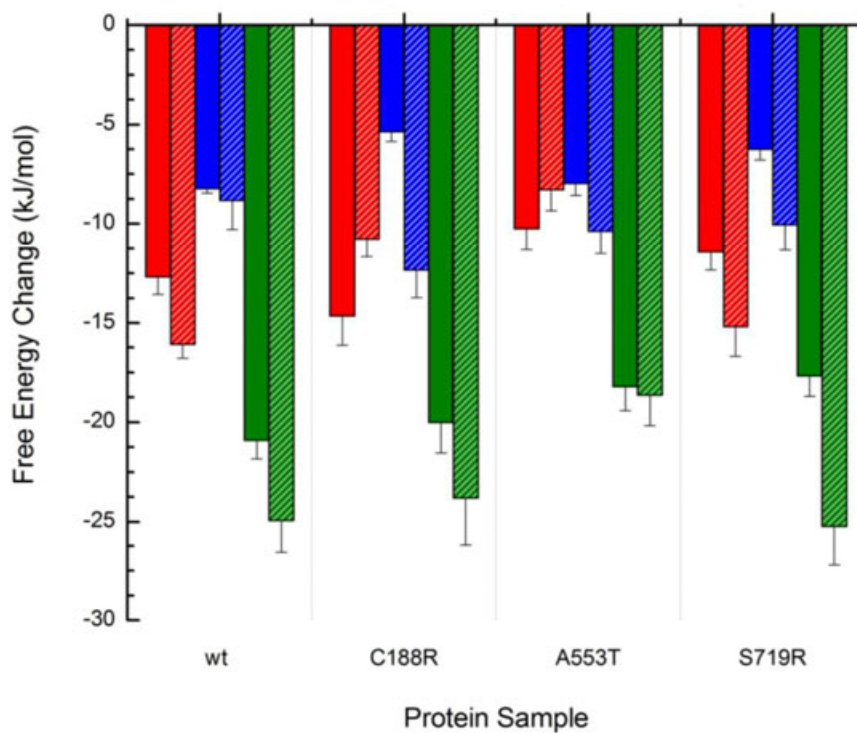
Figure 3. (A) Intensity-weighted average emission wavelength change *versus* guanidine hydrochloride (GdmCl) concentration plots for wild type and mutant PLCδ1 proteins, in the absence (blue) and presence (red) of Ca^{2+}. Data points represent the mean values of four different sample measurements (n=4) at identical GdmCl concentrations, while error bars represent the corresponding standard error of the mean. Solid lines represent non-linear least-squares fit of a two-step unfolding model for fluorescence data. **(B)** Free energy change profiles for the GdmCl-induced unfolding of wild type and mutant proteins derived from the non-linear least-squares fit of a two-step unfolding model for the experimental data in the absence (solid bars) and presence (striped bars) of Ca^{2+}. Red, blue and green bars represent the energy barrier between native and intermediate, intermediate and unfolded, and native and unfolded states, respectively. Error bars represent the standard error of the free energy change calculations.
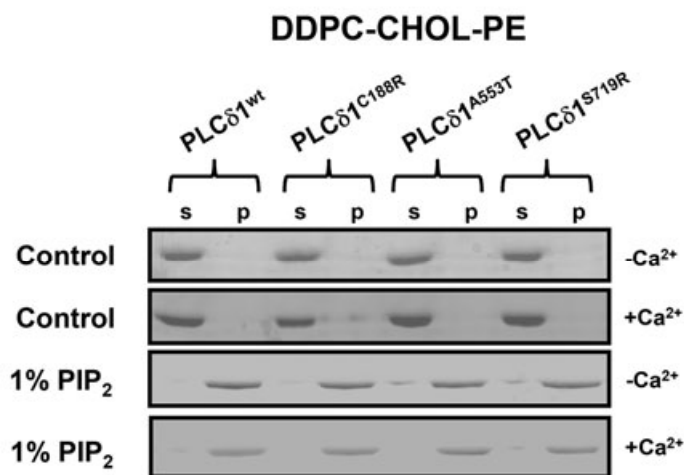

Figure 4. Liposome pull-down assays of wild type and mutant PLCδ1. Unilamellar liposomes comprising PtdCho:CHOL:PtdEtn (4:2:1) with or without 1% w/w PIP_2 were incubated in the presence of 0.5 mM Mg^{2+} with the various purified PLCδ1 recombinant proteins in the presence of either 1 mM EDTA or 1mM $CaCl_2$. Following centrifugation, both the supernatant (s) and pellet (p) were subjected to SDS–PAGE and Coomassie Brilliant Blue staining.
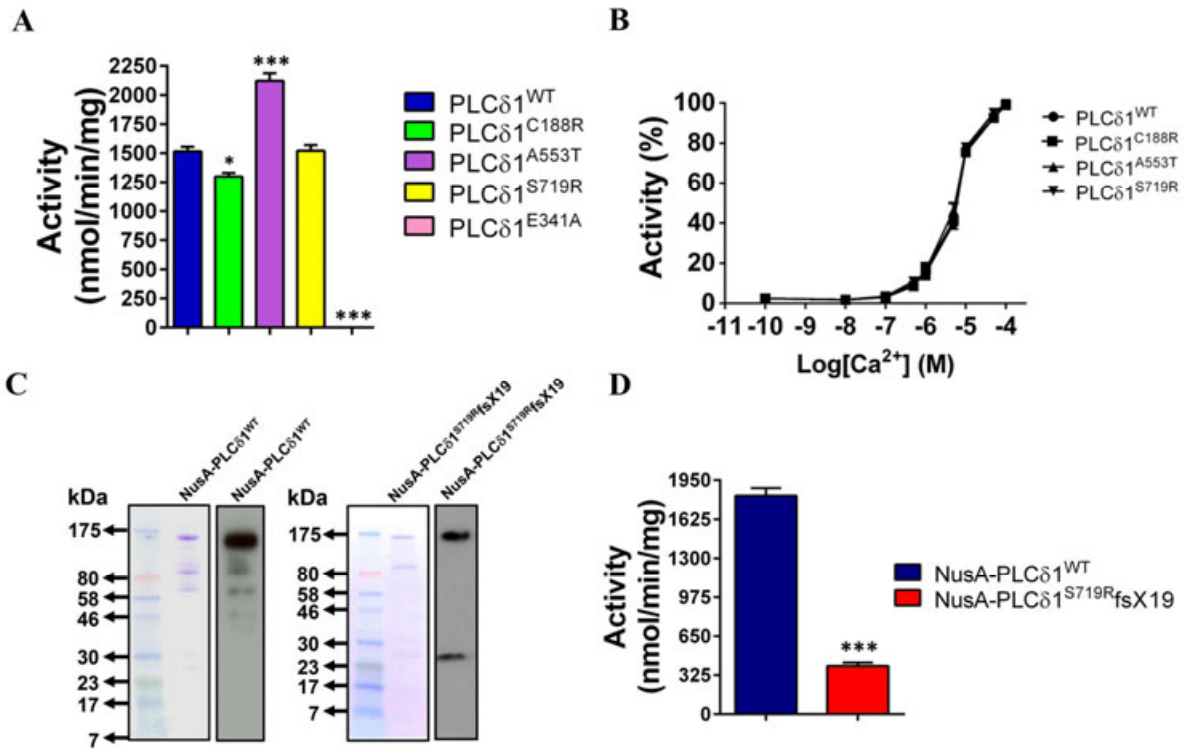
Figure 5. (A) Enzyme activity of PLCδ1 mutants. PIP$_2$ hydrolysis enzyme activities of the purified PLCδ1 proteins were determined (n=4±SEM), using two different preparations of recombinant protein, *p< 0.05; ***p<0.0005. **(B)** Effect of calcium concentration on the normalized activity of wild type PLCδ1 and mutant proteins (n=4±SEM, two different preparations of recombinant protein). **(C)** Affinity-purified NusA-6xHis-PLCδ1 fusion proteins (1 µg) were analysed by SDS-PAGE followed by either Coomassie Brilliant Blue staining (left panels) or immunoblot analysis (right panels). **(D)** [^{3}H]PIP$_2$ hydrolysis activities of the purified NusA-6xHis-PLCδ1 fusion proteins (n=4±SEM, two different preparations of recombinant protein, ***p< 0.0005). In control experiments with NusA alone, no specific PIP$_2$ hydrolysis activity was observed (data not shown).
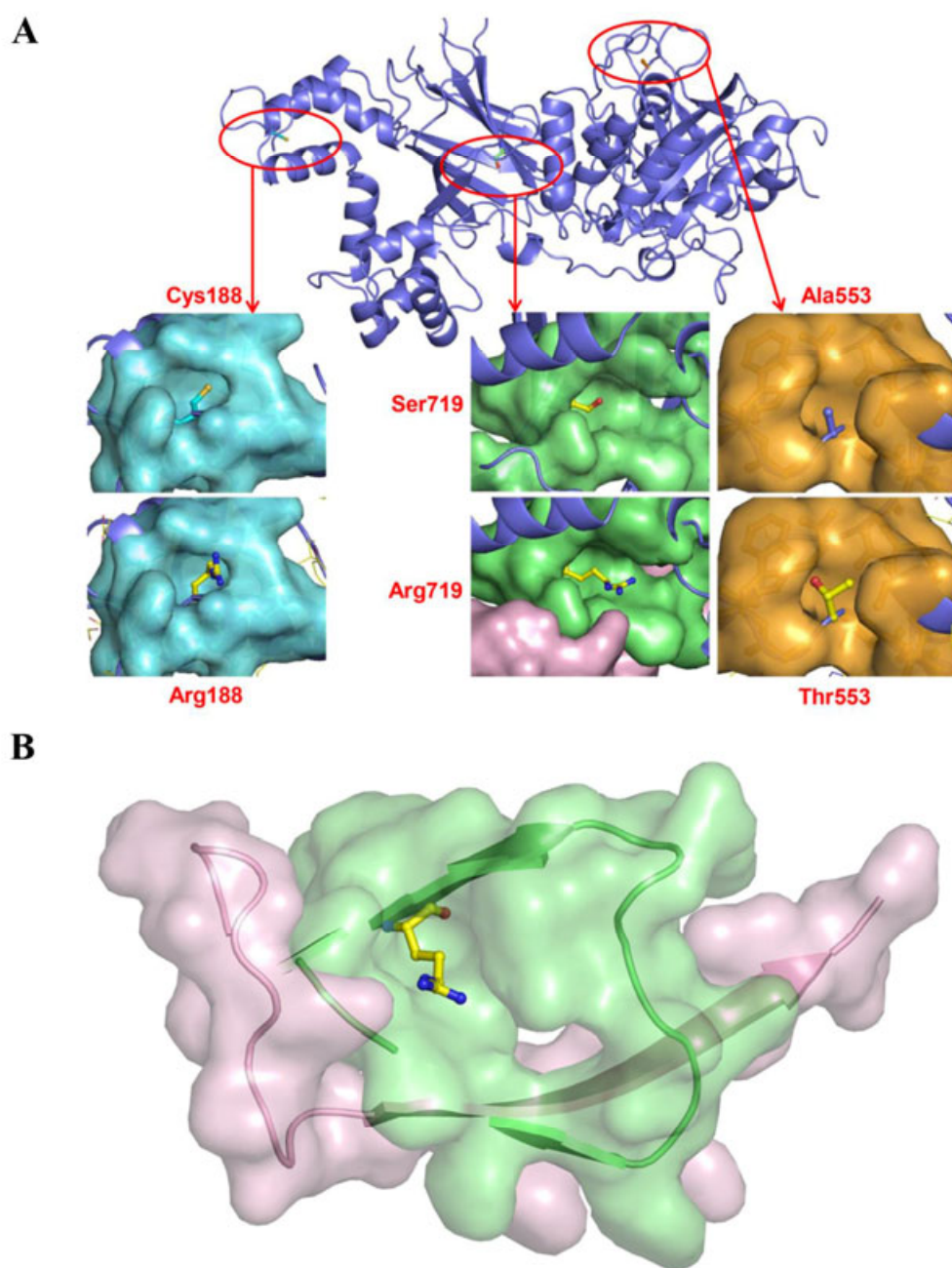
Figure 6. A. Overall structural fold of rat PLCδ1 with the three sites of mutation indicated in ovals. Arrows lead to a magnified image of each site. Central residues are represented as stick models, with the surrounding environment shown as a solid surface at the van der Waals radius. The region around the mutated S719R also indicates the last 19 residues of the chain (738 to 756), in light pink, which were truncated in one construct. **B.** Full extent of the region around the S719R mutation, including the last 19 amino-acid truncation (light pink).